Supporting Information

Low-Temperature Liquid-Crystalline Nitroxide Radical

Yoshiaki Uchida,[*a] Takuya Akita,[a] Takuo Ohkochi,[b,c,d] Xiao-Qian Ma,[a] Daichi Kiyohara,[a] Sho Nakagami,[a] Taira Yamazaki[a] and Norikazu Nishiyama[a]

[a.] *Graduate School of Engineering Science, Osaka University, 1-3 Machikaneyama-cho, Toyonaka, Osaka 560-8531, Japan. E-mail: y.uchida.es@osaka-u.ac.jp*

[b.] *Laboratory of Advanced Science and Technology for Industry, University of Hyogo, Kamigori, Hyogo 678-1205, Japan.*

[c.] *Japan Synchrotron Radiation Research Institute, Sayo, Hyogo 679-5198, Japan.*

[d.] *RIKEN SPring-8 Center, Sayo, Hyogo 679-5148, Japan*

Experimental Procedures

<u>Synthesis methods</u>

General Method for Preparation of TBDMS-protected Bromophenol Derivatives (2)

Fluorinated and non-fluorinated *tert*-butylchlorodimethylsilane (TBDMS)-protected bromophenols **2** were prepared by the similar procedure reported previously.[53]   Imidazole (250 mmol) and *tert*-butyldimethylchlorosilane (TBDMS-Cl, 100 mmol) were added to a solution of fluorinated or non-fluorinated *p*-bromophenol **1** (100 mmol) in *N,N*-dimethylformamide (DMF, 120 mL). The reaction solution was stirred under N_2 atmosphere for 3 hours at room temperature, and then, the reaction was quenched with the addition of saturated aqueous $NaHCO_3$ solution (200 mL). The mixture was extracted with hexane (200 mL × 3) and washed with 1 mol/L aqueous NaOH solution (100 mL) and saturated aqueous NaCl solution (200 mL), and then dried with Na_2SO_4. The crude product was passed through a short pad of silica gel with hexane as eluent to remove unreacted substances and byproducts, and the solvent was evaporated to afford **2** as colorless oil in 95% yield. Traces of the DMF and water were completely eliminated in vacuo for the next step.

General Method for Preparation of Alkoxy Bromobenzene Derivatives (5)

Fluorinated and non-fluorinated alkoxy bromobenzenes **5** were prepared by a similar procedure reported previously.[54] Fluorinated or non-fluorinated *p*-bromophenol **4** (100 mmol) and K_2CO_3 (200 mmol) were dissolved in DMF (150 mL) and stirred 1 hour at 60 °C under N_2 atmosphere. The corresponding iodoalkane (100 mmol) was added to the reaction solution. The reaction was continued overnight. Then, it was cooled to room temperature and added saturated aqueous $NaHCO_3$ solution (200 mL). The organic phase was extracted with hexane (200 mL × 3). The extracts were washed with 1 mol/L aqueous NaOH solution (100 mL) and saturated aqueous NaCl solution (200 mL) and dried with Na_2SO_4. The brown crude oil was passed through a short pad of silica gel with hexane as eluent to remove unreacted substances and byproducts, and the solvent was evaporated to afford **5** as colorless oil in 95% yield. Traces of the DMF and water were completely eliminated in vacuo for the next step.

General Method for Preparation of Grignard Reagents (3 and 6)

Fluorinated and non-fluorinated Grignard reagents **3** and **6** were prepared according to the previously reported procedure.[55] Magnesium turnings (30 mmol) and anhydrous LiCl (33 mmol) were placed and heated in vacuo for 2 hours to eliminate traces of water, and then, dehydrated THF (5 mL) and a small amount of iodine were added under N_2 atmosphere. A solution of aryl bromide **2** or **5** (30 mmol) in dehydrated THF (25 mL) was slowly added at room temperature. The reaction started within a few minutes. After the start of the reaction, the reaction

mixture was stirred for 3 hours at 0 °C. The gray solution of Grignard reagent 3 or 6 was used without further purification.

General Method for Preparation of TBDMS-protected NRs (9)

Racemates of NRs **9** were synthesized by a similar procedure reported previously.[56] According to the previously reported procedure, a racemate of nitrone **7** (20 mmol) was prepared by reducing (±)-5-nitrohexan-2-one with zinc and NH_4Cl.[57] To a stirred solution of the freshly prepared Grignard reagent **3** (~30 mmol) in THF (30 mL) was slowly added a solution of the nitrone **7** (20 mmol) in THF (20 mL) under N_2 at 0 °C. Stirring was continued overnight, and then, the temperature was raised slowly to room temperature. The reaction mixture was poured into a saturated aqueous NH_4Cl solution (50 mL) and extracted with CH_2Cl_2 (50 mL × 2). The combined CH_2Cl_2 extract was dried over Na_2SO_4 and evaporated. The residual oil was dissolved in methanol (160 mL). To this solution were added aqueous NH_3 solution (28 wt%, 6 ml) and copper (II) acetate monohydrate (0.64 mmol). The yellow solution was vigorously stirred to be oxidized by O_2 until a blue-green color was developed. The solvent was then removed under reduced pressure and the crude product **8** was dissolved again in CH_2Cl_2 (50 mL). This solution was washed with saturated aqueous $NaHCO_3$ solution (50 mL), dried over Na_2SO_4, and evaporated. The water was removed by the azeotropic method with benzene and the remaining trace of benzene was removed in vacuo.

To a stirred solution of the crude product **8** in THF (20 mL) was slowly added a solution of the freshly prepared Grignard reagent **6** (~30 mmol) in THF (30 mL) under N_2 at −78 °C. After a similar workup procedure, the crude product was again oxidized by O_2 with additional CH_2Cl_2 as a cosolvent. Purification by column chromatography (hexane to hexane and diethyl ether) on silica gel provided the crude NRs **9** as a yellow oil.

General Method for Deprotection to Afford Phenolic NRs (10)

Racemates of TBDMS-protected NRs **9** were deprotected by the same procedure reported previously.[58] To the crude NR **9** dissolved in THF (200 mL) was added 5 mL of tetrabutylammonium fluoride (TBAF, 1 mol/L solution in THF) at 0 °C. After stirring for 60 min, the mixture was poured into a saturated aqueous NH_4Cl solution (50 mL) and extracted with diethyl ether (Et_2O, 50 mL × 2). The combined organic phase was washed with saturated aqueous NH_4Cl solution (50 mL × 2), dried by $MgSO_4$ and evaporated in vacuo. The residue was purified by column chromatography on silica gel (hexane/2-propanol) and recrystallized from hexane and ethanol to afford **10** as yellow crystals in about 20% yield from nitrone **7**.

General Method for Chiral Resolution of Phenolic Precursors (10)

The racemate of **10** was separated by using HPLC with a chiral column (Daicel Corp., CHIRALCEL OD-H, 20 mm × 250 mm, particle size is 5 μm), a mixture of hexane and 2-propanol (9/1) as a mobile phase and flow rate of 20 mL/min at room temperature. The separated eluent was evaporated to obtain (2*S*,5*S*) and (2*R*,5*R*) enantiomers of **10** as more than 99% enantiomeric excess (*ee*).

General Method for Esterification to Give LC-NRs

The racemic and enantiomerically enriched (2*S*,5*S*) or (2*R*,5*R*) phenolic NR compounds **10** were esterified with corresponding benzoic acid **11** to afford LC-NRs as the final product. Dichloromethane (5 mL) was charged with **10** (0.30 mmol), the benzoic acid **11** (0.33 mmol), 1-(3-dimethylaminopropyl)-3-ethylcarbodiimide hydrochloride (EDC·HCl, 0.45 mmol) and 4-(dimethylamino)pyridine (DMAP, 0.09 mmol). The reaction mixture was stirred at room temperature till the completion of the reaction while tracking the reaction by HPLC analyses. After that, the reaction solution was added to saturated aqueous NaHCO$_3$ solution (50 mL) and extracted with Et$_2$O (50 mL × 2). The extract was washed with saturated aqueous NaHCO$_3$ solution (50 mL) and saturated aqueous NaCl solution (50 mL), dried over Na$_2$SO$_4$ and concentrated in vacuo. The residue was purified by column chromatography on silica gel (hexane/2-propanol) and recrystallized from hexane and ethanol to afford the LC-NRs as yellow crystals in 60–90% yield.

(±)-**8NOF8**: IR (KBr) cm^{-1}: 2924, 2853, 1726, 1607, 1512, 1298, 1248, 1167, 766; HRMS (FAB+) m/z: [M]$^+$ calcd for C$_{41}$H$_{55}$FNO$_5$: 660.4064; found: 660.4068; Anal. calcd for C$_{41}$H$_{55}$FNO$_5$: C, 74.51; H, 8.39; N, 2.12; found: C, 74.57; H, 8.64; N, 2.06; EPR (THF): g = 2.0059, a_N = 1.32 mT; SQUID (0.5 T): C = 0.371 emu K mol^{-1}, θ = −0.154 K.

(±)-**8NOFC8**: IR (KBr) cm^{-1}: 2924, 2855, 1728, 1611, 1510, 1369, 1248, 1180, 831; HRMS (FAB+) m/z: [M]$^+$ calcd for C$_{42}$H$_{57}$FNO$_4$: 658.4272; found: 658.4270; Anal. calcd for C$_{42}$H$_{57}$FNO$_4$: C, 76.56; H, 8.72; N, 2.13; found: C, 76.56; H, 8.98; N, 2.13; EPR (THF): g = 2.0059, a_N = 1.32 mT; SQUID (0.5 T): C = 0.374 emu K mol^{-1}, θ = −0.188 K.

(±)-**8NOFCN**: IR (KBr) cm^{-1}: 2924, 2868, 2232, 1736, 1611, 1510, 1298, 1248, 1184, 760; HRMS (FAB+) m/z: [M]$^+$ calcd for C$_{34}$H$_{38}$FN$_2$O$_4$: 557.2816; found: 557.2818; Anal. calcd for C$_{34}$H$_{38}$FN$_2$O$_4$: C, 73.23; H, 6.87; N, 5.02; found: C, 73.33; H, 6.91; N, 4.99; EPR (THF): g = 2.0059, a_N = 1.32 mT; SQUID (0.5 T): C = 0.387 emu K mol^{-1}, θ = −0.453 K.

(±)-**8FNO7**: IR (KBr) cm^{-1}: 2930, 2857, 1728, 1622, 1504, 1261, 1206, 1171, 1121, 1070, 947, 885, 849, 766, 648; HRMS (FAB+) m/z: [M]$^+$ calcd for C$_{40}$H$_{53}$FNO$_5$: 646.3908; found: 646.3914; Anal. calcd for C$_{40}$H$_{53}$FNO$_5$: C, 74.27; H, 8.26; N, 2.17; found: C, 74.11; H, 8.45; N, 2.16; EPR

(THF): $g = 2.0061$, $a_N = 1.32$ mT; SQUID (0.5 T): $C = 0.363$ emu K mol^{-1}, $\theta = 0.047$ K.

(±)-**8FNO8**: IR (KBr) cm^{-1}: 2924, 2855, 1724, 1605, 1503, 1267, 1204, 1165, 1074, 962, 847, 768; HRMS (FAB+) m/z: [M]$^+$ calcd for C$_{41}$H$_{55}$FNO$_5$: 660.4064; found: 660.4064; Anal. calcd for C$_{41}$H$_{55}$FNO$_5$: C, 74.51; H, 8.39; N, 2.12; found: C, 74.29; H, 8.54; N, 2.12; EPR (THF): $g = 2.0060$, $a_N = 1.32$ mT; SQUID (0.5 T): $C = 0.390$ emu K mol^{-1}, $\theta = 0.021$ K.

(±)-**10FNO10**: IR (KBr) cm^{-1}: 2922, 2855, 1722, 1605, 1501, 1265, 1165, 1072, 1018, 829, 768; HRMS (FAB+) m/z: [M]$^+$ calcd for C$_{45}$H$_{63}$FNO$_5$: 716.4690; found: 716.4688; Anal. calcd for C$_{45}$H$_{63}$FNO$_5$: C, 75.38; H, 8.86; N, 1.95; found: C, 75.49; H, 9.06; N, 1.92; EPR (THF): $g = 2.0061$ $a_N = 1.32$ mT; SQUID (5 T): $C = 0.381$ emu K mol^{-1}, $\theta = -0.160$ K.

(±)-**12FNO12**: IR (KBr) cm^{-1}: 2922, 2853, 1734, 1506, 1256, 1206, 1171, 1078, 847, 764; HRMS (FAB+) m/z: [M]$^+$ calcd for C$_{49}$H$_{71}$FNO$_5$: 772.5316; found: 772.5314; Anal. calcd for C$_{49}$H$_{71}$FNO$_5$: C, 76.13; H, 9.26; N, 1.81; found: C, 76.16; H, 9.22; N, 1.83; EPR (THF): $g = 2.0061$, $a_N = 1.32$ mT; SQUID (0.5 T): $C = 0.397$ emu K mol^{-1}, $\theta = 0.036$ K.

(2*S*,5*S*)-**8NOF8**: IR (KBr) cm^{-1}: 2924, 2855, 1730, 1607, 1512, 1244, 1169, 1049, 762; HRMS (FAB+) m/z: [M]$^+$ calcd for C$_{41}$H$_{55}$FNO$_5$: 660.4064; found: 660.4068; Anal. calcd for C$_{41}$H$_{55}$FNO$_5$: C, 74.51; H, 8.39; N, 2.12; found: C, 74.70; H, 8.64; N, 2.11; EPR (THF): $g = 2.0059$, $a_N = 1.32$ mT; SQUID (5 T): $C = 0.395$ emu K mol^{-1}, $\theta = -0.545$ K.

(2*R*,5*R*)-**8FNO6**: IR (KBr) cm^{-1}: 2930, 2857, 1732, 1607, 1506, 1265, 1209, 1167, 1063, 766; HRMS (FAB+) m/z: [M]$^+$ calcd for C$_{39}$H$_{51}$FNO$_5$: 632.3751; found: 632.3755; Anal. calcd for C$_{39}$H$_{51}$FNO$_5$: C, 74.02; H, 8.12; N, 2.21; found: C, 73.96; H, 7.93; N, 2.22; EPR (THF): $g = 2.0061$, $a_N = 1.32$ mT; SQUID (0.5 T): $C = 0.373$ emu K mol^{-1}, $\theta = -0.053$ K.

(2*S*,5*S*)-**8FNO7**: IR (KBr) cm^{-1}: 2932, 2857, 1734, 1607, 1506, 1256, 1209, 1167, 1070, 1018, 849, 764; HRMS (FAB+) m/z: [M]$^+$ calcd for C$_{40}$H$_{53}$FNO$_5$: 646.3908; found: 646.3907; Anal. calcd for C$_{40}$H$_{53}$FNO$_5$: C, 74.27; H, 8.26; N, 2.17; found: C, 74.24; H, 8.11; N, 2.16; EPR (THF): $g = 2.0061$, $a_N = 1.32$ mT; SQUID (0.5 T): $C = 0.393$ emu K mol^{-1}, $\theta = -0.136$ K.

(2*R*,5*R*)-**8FNO8**: IR (KBr) cm^{-1}: 2924, 2855, 1732, 1605, 1506, 1254, 1204, 1169, 1072, 849, 766; HRMS (FAB+) m/z: [M]$^+$ calcd for C$_{41}$H$_{55}$FNO$_5$: 660.4064; found: 660.4067; Anal. calcd for C$_{41}$H$_{55}$FNO$_5$: C, 74.51; H, 8.39; N, 2.12; found: C, 74.48; H, 8.40; N, 2.14; EPR (THF): $g = 2.0061$, $a_N = 1.32$ mT; SQUID (5 T): $C = 0.372$ emu K mol^{-1}, $\theta = -0.327$ K.

(2*R*,5*R*)-**8FNO9**: IR (KBr) cm^{-1}: 2938, 2855, 1730, 1506, 1314, 1254, 1206, 1171, 1011, 764; HRMS (FAB+) m/z: [M]$^+$ calcd for C$_{42}$H$_{57}$FNO$_5$: 674.4221; found: 674.4227; Anal. calcd for C$_{42}$H$_{57}$FNO$_5$: C, 74.74; H, 8.51; N, 2.08; found: C, 74.76; H, 8.67; N, 2.07; EPR (THF): $g = 2.0061$, $a_N = 1.32$ mT; SQUID (5 T): $C = 0.388$ emu K mol^{-1}, $\theta = -0.348$ K.

(2*R*,5*R*)-**8FNO10**: IR (KBr) cm^{-1}: 2928, 2855, 1732, 1622, 1605, 1506, 1314, 1254, 1206, 1171, 1074, 1016, 962, 839, 764; HRMS (FAB+) m/z: [M]$^+$ calcd for C$_{43}$H$_{59}$FNO$_5$: 688.4377; found: 688.4377; Anal. calcd for C$_{43}$H$_{59}$FNO$_5$: C, 74.97; H, 8.63; N, 2.03; found: C, 74.96; H, 8.67; N,

2.05; EPR (THF): g = 2.0061, a_N = 1.32 mT; SQUID (5 T): C = 0.389 emu K mol^{-1}, θ = −0.127 K.

(2S,5S)-**10FNO10**: IR (KBr) cm^{-1}: 2926, 2855, 1730, 1604, 1504, 1251, 1163, 1067, 1067, 845, 764; HRMS (FAB+) m/z: [M]$^+$ calcd for C$_{45}$H$_{63}$FNO$_5$: 716.4690; found: 716.4692; Anal. calcd for C$_{45}$H$_{63}$FNO$_5$: C, 75.38; H, 8.86; N, 1.95; found: C, 75.45; H, 9.08; N, 1.91; EPR (THF): g = 2.0061, a_N = 1.33 mT; SQUID (0.5 T): C = 0.347 emu K mol^{-1}, θ = 0.060 K.

(2R,5R)-**12FNO12**: IR (KBr) cm^{-1}: 2922, 2853, 1738, 1607, 1506, 1472, 1373, 1258, 1207, 1169, 1148, 1123, 1074, 845, 764; HRMS (FAB+) m/z: [M]$^+$ calcd for C$_{49}$H$_{71}$FNO$_5$: 772.5316; found: 772.5314; Anal. calcd for C$_{49}$H$_{71}$FNO$_5$: C, 76.13; H, 9.26; N, 1.81; found: C, 76.11; H, 9.55; N, 1.80; EPR (THF): g = 2.0060, a_N = 1.32 mT; SQUID (5 T): C = 0.395 emu K mol^{-1}, θ = −0.175 K.

(±)-**8NO(3F)7**: IR (KBr) cm^{-1}: 2920, 2855, 1742, 1605, 1510, 1254, 1167, 762; HRMS (FAB+) m/z: [M]$^+$ calcd for C$_{40}$H$_{53}$FNO$_5$: 646.3908; found: 646.3911; Anal. calcd for C$_{40}$H$_{53}$FNO$_5$: C, 74.27; H, 8.26; N, 2.17; found: C, 74.39; H, 8.02; N, 2.16; EPR (THF): g = 2.0059, a_N = 1.33 mT; SQUID (5 T): C = 0.400 emu K mol^{-1}, θ = −0.258 K.

(±)-**8NO(3F5F)7**: IR (KBr) cm^{-1}: 2930, 2859, 1740, 1605, 1514, 1258, 1215, 1169, 1043; HRMS (FAB+) m/z: [M]$^+$ calcd for C$_{40}$H$_{52}$F$_2$NO$_5$: 664.3814; found: 664.3807; Anal. calcd for C$_{40}$H$_{52}$F$_2$NO$_5$: C, 72.26; H, 7.88; N, 2.11; found: C, 72.33; H, 7.97; N, 2.11; EPR (THF): g = 2.0059, a_N = 1.33 mT; SQUID (5 T): C = 0.386 emu K mol^{-1}, θ = −0.234 K.

(±)-**8NO(2F5F)7**: IR (KBr) cm^{-1}: 2922, 2855, 1748, 1605, 1512, 1256, 1169, 1067, 762; HRMS (FAB+) m/z: [M]$^+$ calcd for C$_{40}$H$_{52}$F$_2$NO$_5$: 664.3814; found: 664.3807; Anal. calcd for C$_{40}$H$_{52}$F$_2$NO$_5$: C, 72.26; H, 7.88; N, 2.11; found: C, 72.14; H, 7.65; N, 2.06; EPR (THF): g = 2.0059, a_N = 1.32 mT; SQUID (5 T): C = 0.371 emu K mol^{-1}, θ = −0.440 K.

(±)-**8NO(3F)C7**: IR (KBr) cm^{-1}: 2928, 2855, 1740, 1609, 1510, 1261, 1180, 1067, 831; HRMS (FAB+) m/z: [M]$^+$ calcd for C$_{41}$H$_{55}$FNO$_4$: 644.4115; found: 644.4120; Anal. calcd for C$_{41}$H$_{55}$FNO$_4$: C, 76.36; H, 8.60; N, 2.17; found: C, 76.46; H, 8.81; N, 2.18; EPR (THF): g = 2.0059, a_N = 1.33 mT; SQUID (5 T): C = 0.387 emu K mol^{-1}, θ = −0.446 K.

(±)-**8NO(3F5F)C7**: IR (KBr) cm^{-1}: 2928, 2855, 1753, 1607, 1510, 1252, 1217, 1179, 1040; HRMS (FAB+) m/z: [M]$^+$ calcd for C$_{41}$H$_{54}$F$_2$NO$_4$: 662.4021; found: 662.4020; Anal. calcd for C$_{41}$H$_{54}$F$_2$NO$_4$: C, 74.29; H, 8.21; N, 2.11; found: C, 74.23; H, 8.29; N, 2.12; EPR (THF): g = 2.0059, a_N = 1.33 mT; SQUID (5 T): C = 0.389 emu K mol^{-1}, θ = −0.305 K.

(±)-**8NO(2F5F)C7**: IR (KBr) cm^{-1}: 2924, 2853, 1761, 1611, 1508, 1250, 1175, 1013, 756; HRMS (FAB+) m/z: [M]$^+$ calcd for C$_{41}$H$_{54}$F$_2$NO$_4$: 662.4021; found: 662.4023; Anal. calcd for C$_{41}$H$_{54}$F$_2$NO$_4$: C, 74.29; H, 8.21; N, 2.11; found: C, 74.37; H, 8.42; N, 2.18; EPR (THF): g = 2.0059, a_N = 1.32 mT; SQUID (5 T): C = 0.392 emu K mol^{-1}, θ = −0.100 K.

(±)-**8NO(3F)CN**: IR (KBr) cm^{-1}: 2924, 2855, 2232, 1753, 1609, 1512, 1263, 1067, 831, 762;

HRMS (FAB+) m/z: [M]$^+$ calcd for $C_{34}H_{38}FN_2O_4$: 557.2816; found: 557.2814; Anal. calcd for $C_{34}H_{38}FN_2O_4$: C, 73.23; H, 6.87; N, 5.02; found: C, 73.33; H, 6.91; N, 4.99; EPR (THF): $g =$ 2.0059, $a_N = 1.33$ mT; SQUID (5 T): $C = 0.393$ emu K mol^{-1}, $\theta = -0.100$ K.

(±)-**8NO(3F5F)CN**: IR (KBr) cm^{-1}: 2924, 2857, 2232, 1753, 1605, 1510, 1263, 1211, 1180, 1042; HRMS (FAB+) m/z: [M]$^+$ calcd for $C_{34}H_{37}F_2N_2O_4$: 575.2721; found: 575.2720; Anal. calcd for $C_{34}H_{37}F_2N_2O_4$: C, 70.94; H, 6.48; N, 4.87; found: C, 70.74; H, 6.53; N, 4.80; EPR (THF): $g =$ 2.0059, $a_N = 1.33$ mT; SQUID (5 T): $C = 0.396$ emu K mol^{-1}, $\theta = -0.100$ K.

(±)-**8NO(2F5F)CN**: IR (KBr) cm^{-1}: 2926, 2855, 2230, 1753, 1609, 1510, 1263, 1177, 1018, 758; HRMS (FAB+) m/z: [M]$^+$ calcd for $C_{34}H_{37}F_2N_2O_4$: 575.2721; found: 575.2719; Anal. calcd for $C_{34}H_{37}F_2N_2O_4$: C, 70.94; H, 6.48; N, 4.87; found: C, 70.81; H, 6.39; N, 4.80; EPR (THF): $g =$ 2.0059, $a_N = 1.32$ mT; SQUID (5 T): $C = 0.394$ emu K mol^{-1}, $\theta = -0.630$ K.

Characterization methods

Determination of ee Value of LC-NRs

HPLC analyses were carried out using a chiral stationary phase column (Daicel Corp., CHIRALCEL OD-H, 4.6 mm × 250 mm, particle size is 5 μm) at 40 °C, a mixture of hexane and 2-propanol (9/1) as the mobile phase at a flow rate of 1 mL/min, and UV spectrometer (254 nm) as a detector. The *ee* value was determined from a ratio of peak area of each enantiomer in the obtained chromatogram.

Thermal Stability of (2*S*,5*S*)-8FNO7

Thermal stability of (2*S*,5*S*)-**8FNO7** was evaluated by thermogravimetric analysis (TGA) in the air. The high thermal stability of (2*S*,5*S*)-**8FNO7** regardless of the radical moiety; (2*S*,5*S*)-**8FNO7** is thermally stable up to about 200 °C in the air.

Determination of X-ray Crystal Structures

Crystals of (2*S*,5*S*)-**8FNO7** suitable for XRD studies were prepared by the recrystallization from ethanol solution and analyzed using an X-ray diffractometer. The X-ray crystal structure of (2*S*,5*S*)-**8FNO7** was solved by direct methods and refined using the full-matrix least-squares method. In subsequent refinements, the function $\sum \omega \left(F_o^2 - F_c^2 \right)^2$ was minimized, where F_o and F_c are the observed and calculated structure factor amplitudes, respectively. The positions of non-hydrogen atoms were determined from difference Fourier electron-density maps and refined anisotropically. All calculations were performed with the Crystal Structure crystallographic software package.

Evaluation of Magnetic Properties from SQUID Magnetometry

The temperature dependence of molar magnetic susceptibility χ_M was measured on an MPMS SQUID magnetometer in the first heating process. Each sample of 5–10 mg was enclosed in a DSC aluminum sample pan to prevent the sign inversion of the total magnetic susceptibility of samples mounted in a drinking straw in high-temperature ranges. The sample was heated from 1.8 to 300 K. We waited for one minute at each temperature to stabilize. The heating rate between the measurement temperatures was 20 K min^{-1}. Curie constant C and Weiss constant θ were evaluated by fitting experimental magnetic susceptibility data with the following equation involving the term of Curie–Weiss law of paramagnetic contribution χ_{para} and small diamagnetic contribution χ_{dia},

$$\chi_M = \chi_{para} + \chi_{dia} = \frac{C}{T - \theta} + \chi_{dia} \, . \tag{8}$$

Derivation of Magnetic Properties from EPR Spectroscopy

The X-band EPR spectra of (2*S*,5*S*)-**8FNO7** in the Cr, LC, and Iso states were observed by using a quartz tube (5 mm ϕ) in a magnetic field of about 0.33 T. Sweep time was 90 s, modulation width was 0.2 mT and time constant was 0.03 s. The heating and cooling rates of our temperature control unit cannot be set, but the rate between the measurement temperatures was 1-3 K min^{-1}. To discuss the weak effects by using accurately measured data, EPR spectra were measured in the narrow range of the magnetic field, and all observed spectra were almost Lorentzian first derivative curves in an ambient temperature range, as shown in Fig. S13. The *g*-value and the linewidth of the EPR spectra were calibrated using a standard Mn^{2+}/MgO marker sample. To evaluate paramagnetic susceptibility from the EPR spectra by the previously reported method,[21] the experimental EPR spectra were fitted with the differential Lorentzian function,

$$\text{(3)}$$

$$I'(H) = -16 I'_m \frac{H - H_0}{\Delta H_{pp}/2} \left[3 + \left(\frac{H - H_0}{\Delta H_{pp}/2} \right)^2 \right]^{-2}$$

where I'_m is the maximum peak height of the differential curve, H is the applied magnetic field, H_0 is the resonant magnetic field, and ΔH_{pp} is the peak-to-peak linewidth. The experimental data can be well fitted with the above-mentioned differential Lorentzian function, as shown in **Fig. S14**. By using the parameters directly obtained from the curve fitting, such as I'_m, ΔH_{pp} and H_0, the paramagnetic susceptibility (χ_{para}) can be evaluated from Bloch equation as follows[21,59,60]

$$\chi_{para} = \frac{2 \mu_B g I'_m \Delta H_{pp}^2}{\sqrt{3} h \nu H_1} \tag{4}$$

where μ_B is Bohr magneton, h is Planck constant, ν is the frequency of the absorbed electromagnetic wave, H_1 is the amplitude of the oscillating magnetic field, and g is the *g*-value,

$$\text{(5)}$$

which is inversely proportional to H_0. For plotting the temperature dependence of χ_{para}, the relative paramagnetic susceptibility χ_{rel}, which is defined as

$$\chi_{rel} = \frac{\chi_{para}}{\chi_0}$$

where χ_0 is the standard paramagnetic susceptibility defined as the value at 30 °C in the first heating process, was used in place of χ_{para} to simplify the treatment. The magnetic data are the mean values of four measurements at each temperature to estimate χ_{para} with high accuracy.

Derivation of Inhomogeneity of Intermolecular Magnetic Interactions from EPR Spectra

The Gaussian component of EPR peak-to-peak linewidth (ΔH_{pp}^{G}) reflects the inhomogeneous broadening of the EPR spectra, which is useful to discuss the influence of the inhomogeneous intermolecular contacts on the magneto-LC effects.[59] Although we fitted the observed EPR spectra with Lorentzian first derivative curve to evaluate paramagnetic susceptibility χ_{para}, it is well-known that EPR spectra are inhomogeneously broadened by the unresolved proton hyperfine coupling and magnetic-field modulation. Hence, the spectra become a Voigtian function, (which is the convolution of Gaussian and Lorentzian functions.[61] The ΔH_{pp}^{G} contains the contribution of Gaussian linewidth in the limit of the zero modulation (ΔH_{pp0}^{G}) and magnetic field modulation (κH_m), where H_m is the modulation amplitude, and κ is a constant.[59] In our case of LC-NRs, the contribution of inhomogeneous intermolecular contacts (H_{IIC}) should be added to the Gaussian component. Therefore, ΔH_{pp}^{G} can be expressed as the root-mean-square of the components.[59,61]

$$\Delta H_{pp}^{G\,2} = \Delta H_{pp0}^{G\,2} + \kappa^2 H_m^{\,2} + H_{IIC}^{\,2}$$
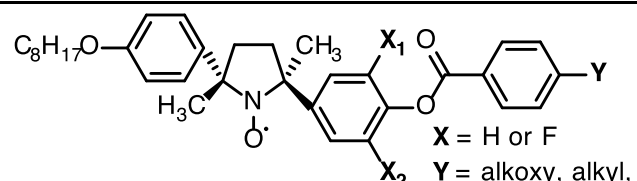
Among the terms, only H_{IIC}^2 depends on temperature. Thus, we can discuss the influence of inhomogeneous intermolecular contacts on the magneto-LC effects by analyzing the temperature dependence of ΔH_{pp}^{G}. We fitted the spectra obtained from the numerical integration of the raw data $I(H)$ with the Voigtian function to estimate ΔH_{pp}^{G} of (2S,5S)-**8FNO7**

$$I(H) = I_V \int \frac{\exp\left[-2(H' - H_0)^2/\Delta H_{pp}^{G\,2}\right]}{1 + \left(\dfrac{H' - H}{\sqrt{3}\Delta H_{pp}^{L}/2}\right)^2}\,dH' \qquad (7)$$
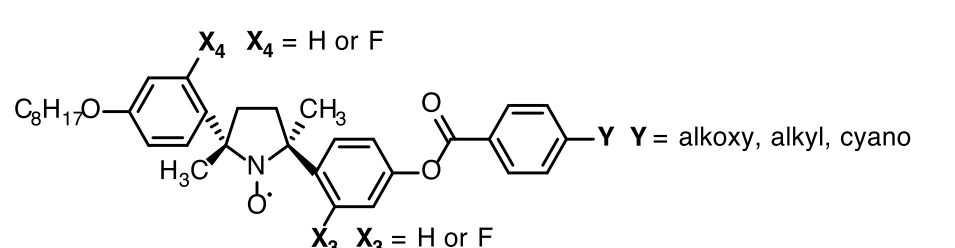
where I_V is a constant, and ΔH_{pp}^{L} is the Lorentzian peak-to-peak linewidth influenced by the magnitude of intermolecular magnetic interactions. The numerical integration of the experimental data $I(H)$ can be better fitted with the above-mentioned Voigtian function than with the differential Lorentzian function. The parameter ΔH_{pp}^{G} was obtained.
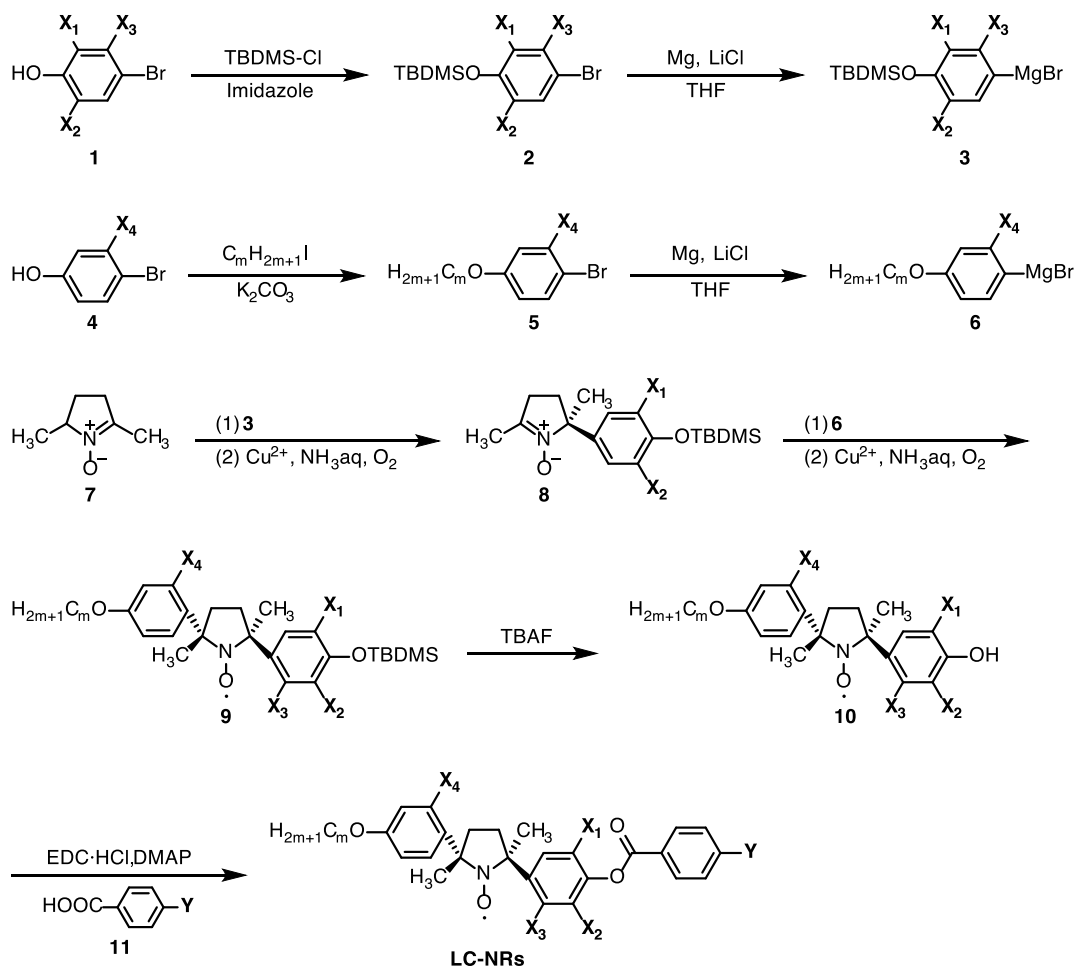
Scheme S1 Synthesis of LC-NRs. C-F bonds were stable during the reactions, including Grignard reactions, deprotection, and esterification.

Table S1 Molecular structures and phase behaviors of new LC-NRs.

X = H or F
Y = alkoxy, alkyl, cyano

Compound				Phase transition temperature [°C]				
Entry	X_1	X_2	Y	Cr		N		Iso
(±)-**8NO7**[28,34]	H	H	OC_7H_{15}	•	78.8	•	106.1	•
(±)-**8NO(3F)7**	F	H	OC_7H_{15}	•	89.5	•	91.7	•
(±)-**8NO(3F5F)7**	F	F	OC_7H_{15}	•	74.1	•	(71.9)	•
(±)-**8NOC7**[34]	H	H	C_8H_{17}	•	79.1	•	(76.5)	•
(±)-**8NO(3F)C7**	F	H	C_8H_{17}	•	83.0	•	(56.4)	•
(±)-**8NO(3F5F)C7**	F	F	C_8H_{17}	•	74.9	•	(34.0)	•
(±)-**8NOCN**[37]	H	H	CN	•	121.2	•	136.2	•
(±)-**8NO(3F)CN**	F	H	CN	•	99.2	•	120.8	•
(±)-**8NO(3F5F)CN**	F	F	CN	•	119.5	•	(95.7)	•

Table S2 Molecular structures and phase behaviors of synthesized LC-NRs.

X_4 = H or F
X_3 = H or F
Y = alkoxy, alkyl, cyano

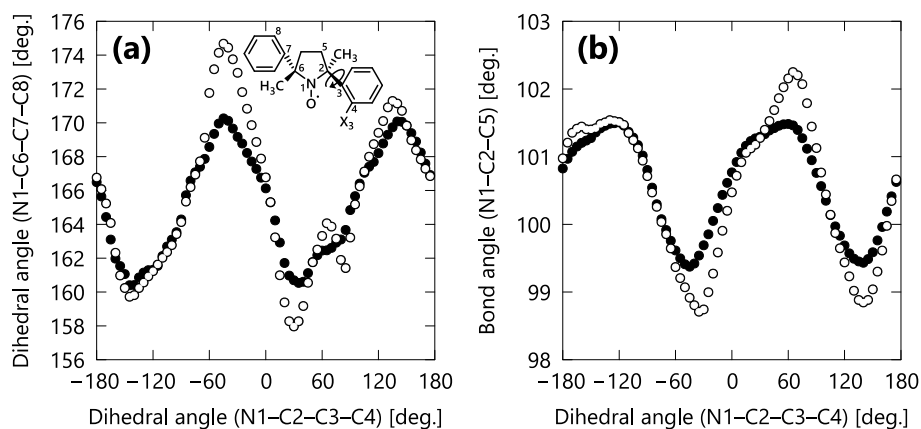| Compound					Phase transition temperature [°C]				
Entry	ee [%]	X_3	X_4	Y	Cr		N		Iso
(±)-**8NO8**[28,34]	0	H	H	OC_8H_{17}	•	73.3	•	104.1	•
(±)-**8NOF8**	0	F	H	OC_8H_{17}	•	68.1	•	79.4	•
(±)-**8FNO8**	0	H	F	OC_8H_{17}	•	78.5	•	82.9	•
(±)-**8NOC8**[34]	0	H	H	C_9H_{19}	•	79.2	•	(77.4)	•
(±)-**8NOFC8**	0	F	H	C_9H_{19}	•	59.1	•	(48.3)	•
(±)-**8NOCN**[37]	0	H	H	CN	•	121.2	•	136.2	•
(±)-**8NOFCN**	0	F	H	CN	•	118.6	•	(117.5)	•
(2S,5S)-**8NO8**[28,34]	>99	H	H	OC_8H_{17}	•	77.8	•	105.3	•
(2S,5S)-**8NOF8**	>99	F	H	OC_8H_{17}	•	52.0	•	77.7	•
(2R,5R)-**8FNO8**	>99	H	F	OC_8H_{17}	•	48.5	•	82.4	•

Fig. S1 Calculation of the correlation between two angles in the same molecule. a) Calculated dihedral angle (N1–C6–C7–C8). b) bond angle (N1–C2–C5) as a function of dihedral angle (N1–C2–C3–C4). Closed and open circles indicate X_3 = H and F, respectively.

Table S3 Molecular structures and phase behaviors of synthesized LC-NRs.

Compound				Phase transition temperature [°C]				
Entry	X_4	m	n	Cr		N		Iso
(±)-**8NO7**[28,34]	H	8	7	•	78.8	•	106.1	•
(±)-**8FNO7**	F	8	7	•	74.3	•	83.5	•
(±)-**8NO8**[28,34]	H	8	8	•	73.3	•	104.1	•
(±)-**8FNO8**	F	8	8	•	78.5	•	82.9	•
(±)-**10NO10**	H	10	10	•	77.3	•	94.1	•
(±)-**10FNO10**	F	10	10	•	77.5	•	(74.8)	•
(±)-**12NO12**	H	12	12	•	71.6	•	80.7	•
(±)-**12FNO12**	F	12	12	•	76.5	•	(72.8)	•
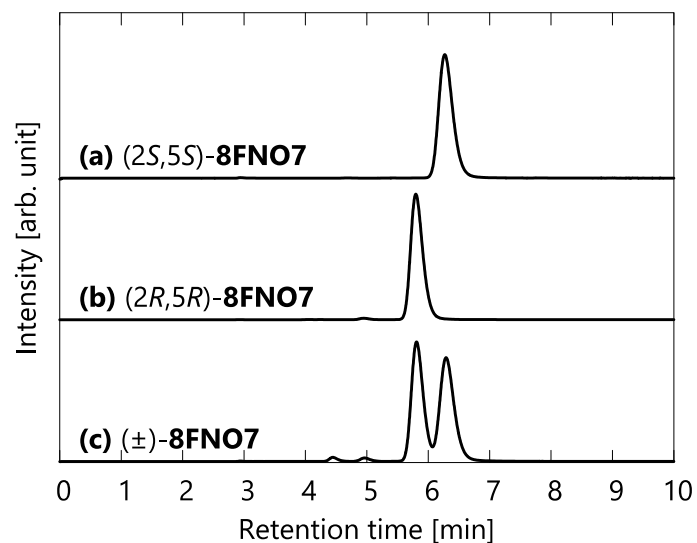
Fig. S2 HPLC chiral chromatograms. a) (2*S*,5*S*)-**8FNO7**. b) (2*R*,5*R*)-**8FNO7**. c) (±)-**8FNO7**.

Table S4 Molecular structures and phase behaviors of *m*FNO*n*.

ee > 99%
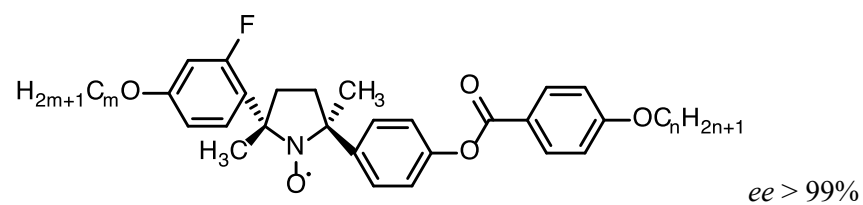
Compound			Phase transition temperature [°C]					
Entry	*m*	*n*	Cr		N*		Iso	
(2*R*,5*R*)-**8FNO6**	8	6	•	51.0	•	88.6	•	
(2*S*,5*S*)-**8FNO7**	8	7	•	36.6	•	80.2	•	
(2*R*,5*R*)-**8FNO8**	8	8	•	48.5	•	82.4	•	
(2*R*,5*R*)-**8FNO9**	8	9	•	60.8	•	78.3	•	
(2*R*,5*R*)-**8FNO10**	8	10	•	61.6	•	78.1	•	
(2*S*,5*S*)-**10FNO10**	10	10	•	56.1	•	75.7	•	
(2*R*,5*R*)-**12FNO12**	12	12	•	60.7	•	73.4	•	
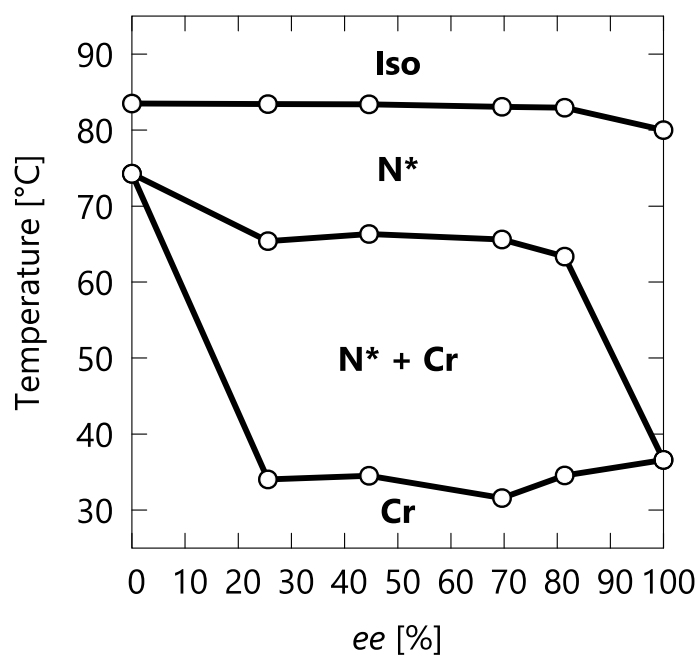
Fig. S3 The *ee*-value dependence of phase behaviors for **8FNO7**. The solid line is a guide for the eye.

Table S5 Crystallographic data of (2*S*,5*S*)-**8FNO7**.

Empirical Formula	$C_{40}H_{53}FNO_5$
Formula Weight	646.86
Crystal Color, Habit	yellow, chip
Crystal Dimensions	0.40 x 0.40 x 0.30 mm
Crystal System	Triclinic
Lattice Parameters	$a = 8.864$ Å
	$b = 14.336$ Å
	$c = 15.518$ Å
	$\alpha = 79.080(8)°$
	$\beta = 82.128(9)°$
	$\gamma = 69.200(6)°$
	$V = 1804.8(3)$ Å^3
Space Group	*P*1
Z value	2
R value	0.0389
wR2 value	0.1070
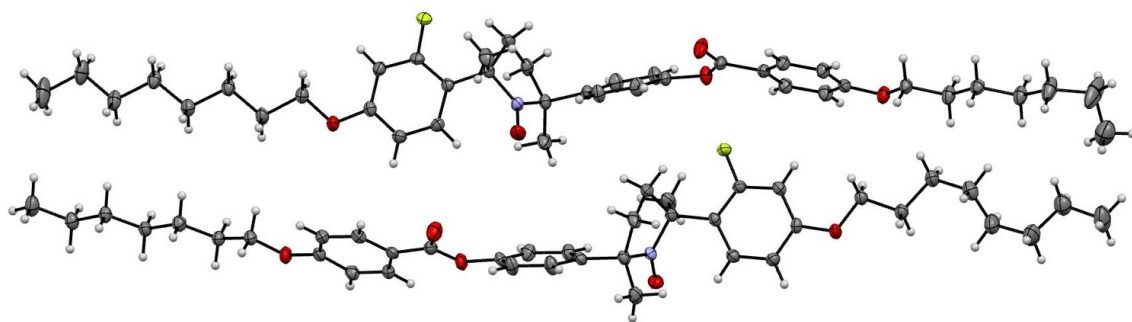
Fig. S4 Crystal structure of (2*S*,5*S*)-**8FNO7** determined by X-ray crystallographic analysis.
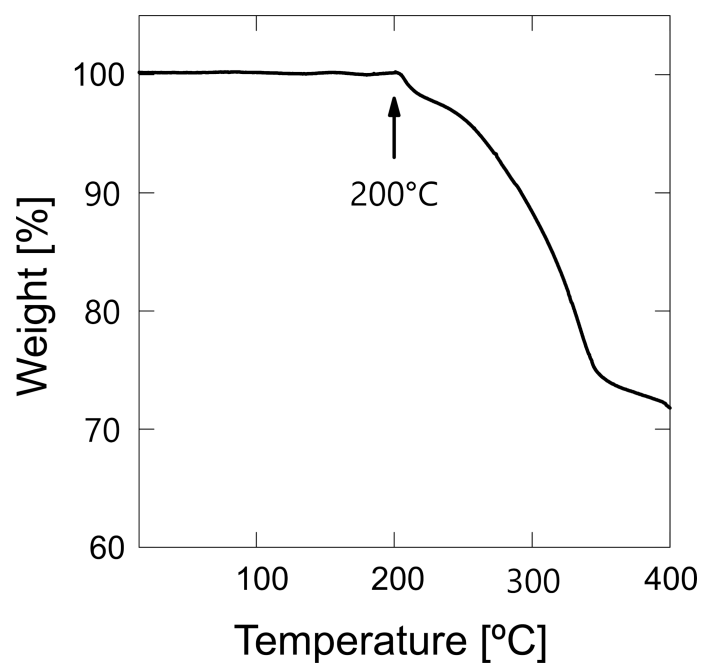
Fig. S5 Thermal stability of (2*S*,5*S*)-**8FNO7**. TGA curve for (2*S*,5*S*)-**8FNO7** at a scanning rate of 2 °C/min in the air. The decomposition seems to start from about 200 °C.
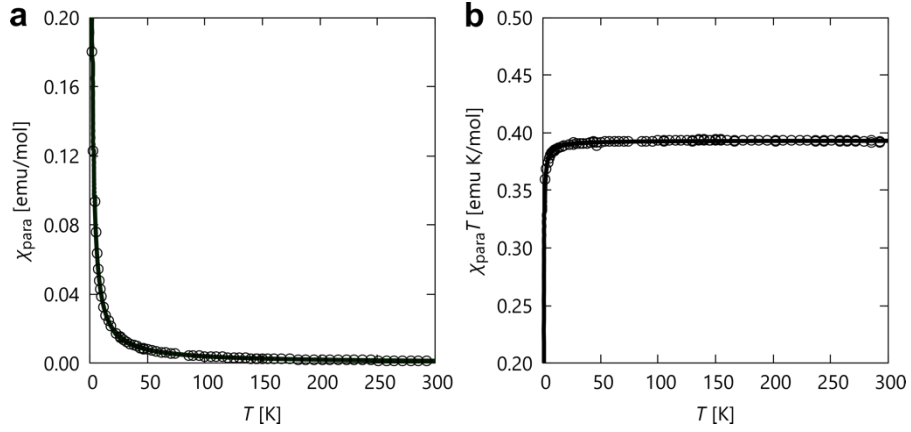
Fig. S6 SQUID magnetometry of (2*S*,5*S*)-**8FNO7** at a field of 0.5 T in the first heating process. a) χ_{para}-T plot. b) $\chi_{\text{para}}T$-T plot. Open circles represent the experimental data, and solid lines show theoretical curves of a) Curie-Weiss law with $C = 0.393$ and $\theta = -0.136$ and of b) Bleaney-Bowers equation for the singlet-triplet model with $\alpha = 1.04$ and $J/k_{\text{B}} = 0.346$.
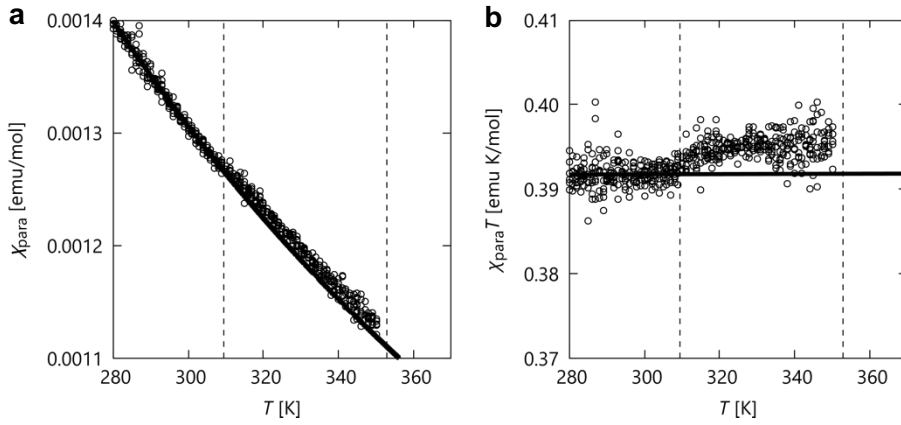
Fig. S7 Temperature dependences of magnetic properties for (2*S*,5*S*)-**8FNO7**. a) χ_{para}-T plots at a magnetic field of 5 T. b) $\chi_{\text{para}}T$-T plots at a magnetic field of 5 T. The circles denote the experimental data in the first heating run, the solid lines denote the Currie-Weiss curve fitted between 280 and 305 K, and the vertical dotted lines denote the Cr-to-N* and N*-to-Iso phase transition temperatures.
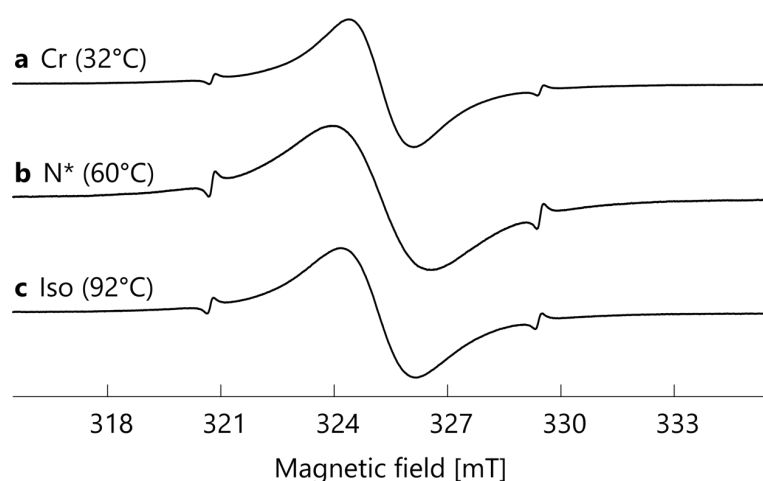
Fig. S8 Selected EPR spectra of (2*S*,5*S*)-**8FNO7**. a) Cr phase at 32 °C in the first heating process. b) N* phase at 60 °C in the first heating process. c) Iso phase at 92 °C in the first heating process.
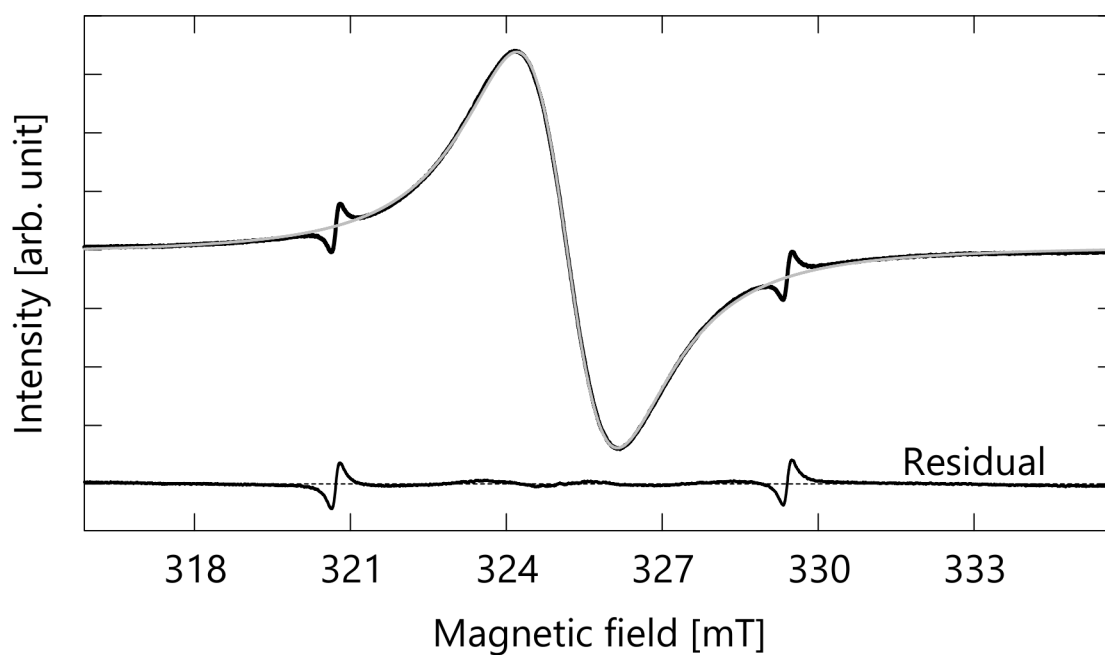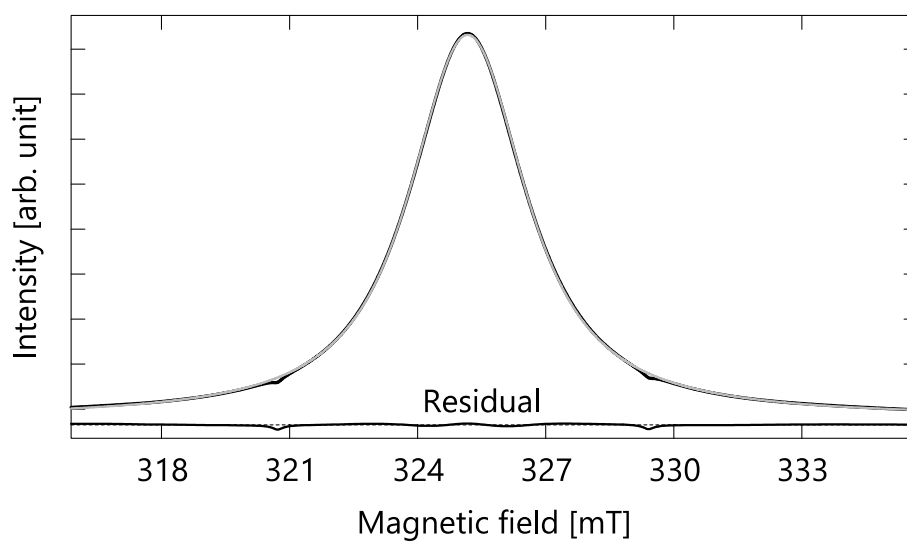

Fig. S9 Selected EPR spectrum of (2*S*,5*S*)-**8FNO7** in Iso phase at 92 °C in the first heating process. Experimental data (black line), a fitted curve of differential Lorentzian function (gray line) and little residuals between them (lower black line) are shown. Dashed horizontal lines mean that the residuals are equal to zero.
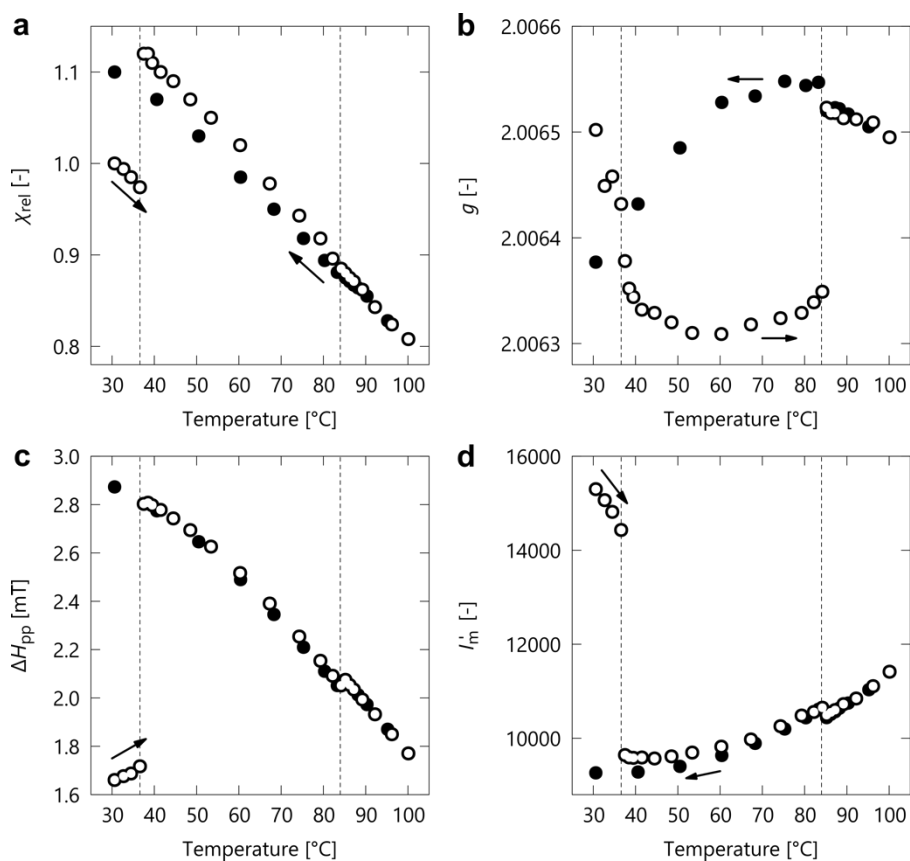
Fig. S10 Selected EPR spectrum in the integral form of (2*S*,5*S*)-**8FNO7** at 92 °C in the first heating process. Experimental data (black line), a fitted curve of Voigtian function (gray line) and little residuals between them (lower black line) are shown. Dashed horizontal lines mean that the residuals are equal to zero.

Fig. S11 Temperature dependence of EPR spectra of (2*S*,5*S*)-**8FNO7** around a field of 0.33 T. a) χ_{rel}. b) *g*-value. c) ΔH_{pp}. d) I'_m. Open and filled circles represent the first heating and cooling processes, respectively. Error bars are not shown because they are sufficiently small. Vertical dotted lines denote the melting points and clearing points expected by DSC analysis and the changes of I'_m in the first heating and cooling processes.
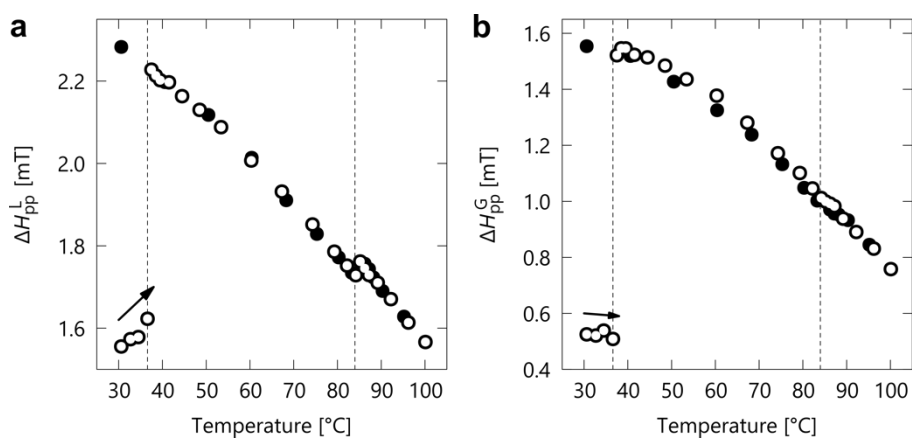
Fig. S12 Temperature dependence of EPR spectra of (2*S*,5*S*)-**8FNO7** around a field of 0.33 T. a) ΔH_{pp}^{L}. b) ΔH_{pp}^{G}. Open and filled circles represent the first heating and cooling processes, respectively. Error bars are not shown because they are sufficiently small. Vertical dotted lines denote the melting points and clearing points expected by DSC analysis and the changes of I'_{m} in the first heating and cooling processes.
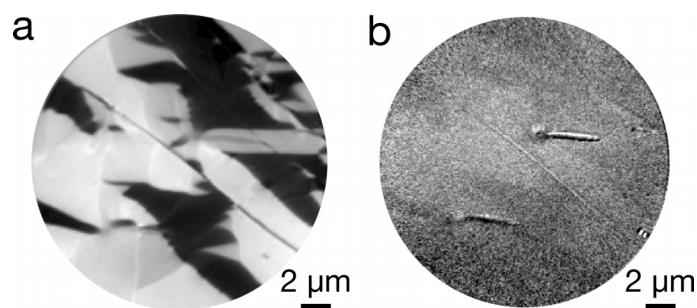

Fig. S13 Measurement of oxygen in a pure Fe film with the top surface oxidized. a) XMCD-PEEM image at the absorption peak of the Fe L_3-edge (708 eV). b) XMCD-PEEM image of the same region of the sample as a) at the absorption peak of the O K-edge (530 eV).
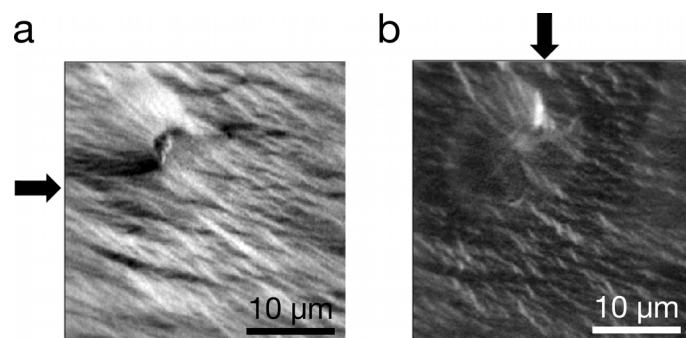
Fig. S14 XMCD-PEEM images of iron-deposited silicon substrate. a) XMCD-PEEM image at the absorption peak of the Fe L_3-edge (708 eV) under the synchrotron radiation from the direction indicated by an arrow. b) XMCD-PEEM image of the same region of the sample as a) at the absorption peak of the Fe L_3-edge (708 eV) under the synchrotron radiation from the direction indicated by an arrow. When the brightness is high, the magnetization direction matches the synchrotron radiation direction. The black area indicates that the magnetization is opposite to the SR direction.

References

53   S. Fujii, Y. Miyajima, H. Masuno and H. Kagechika, *J. Med. Chem.*, 2013, **56**, 160–166.

54   B. Sambathkumar, P. S. V. Kumar, K. Saurav, S. S. K. Iyer, V. Subramanian and N. Somanathan, *New J. Chem.*, 2016, **40**, 3803–3811.

55   A. Krasovskiy and P. Knochel, *Angew. Chem. Int. Ed.*, 2004, **43**, 3333–3336.

56   Y. Uchida, R. Tamura, N. Ikuma, S. Shimono, J. Yamauchi, Y. Aoki and H. Nohira, *Mol. Cryst. Liq. Cryst.*, 2007, **479**, 213/[1251]-221/[1259].

57   E. G. Janzen, Y.-K. Zhang and D. L. Haire, *Magn. Reson. Chem.*, 1994, **32**, 711–720.

58   N. Ikuma, R. Tamura, K. Masaki, Y. Uchida, S. Shimono, J. Yamauchi, Y. Aoki and H. Nohira, *Ferroelectrics*, 2006, **343**, 119–125.

59   Y. Uchida, K. Suzuki and R. Tamura, *J. Phys. Chem. B*, 2012, **116**, 9791–9795.

60   F. Bloch, *Phys. Rev.*, 1946, **70**, 460–474.

61   B. L. Bales, M. Peric and M. T. Lamy-Freund, *J. Magn. Reson.*, 1998, **132**, 279–286.